

Fourier Transformed Spectral Bio-imaging for Studying the Intracellular Fate of Liposomes

Ulrich Huth,^{1*} Ansgar Wieschollek,¹ Yuval Garini,² Rolf Schubert,¹ and Regine Peschka-Süss¹

¹Department of Pharmaceutical Technology, Albert-Ludwigs University, Freiburg, Germany

²Department of Imaging Science and Technology, Delft University of Technology, Delft, The Netherlands

Background: To improve the efficiency of liposomal drug targeting systems, it is necessary to understand the mechanism of liposome uptake by the cell and to follow the intracellular fate of internalized liposomes and their contents.

Methods: We applied multiple-color fluorescence imaging spectroscopy, using a combination of five fluorescent dyes with a significant spectral overlap. pH-sensitive liposomes were labeled with the hydrophilic dye fluorescein isothiocyanate-dextran (FITC-dextran) or the lipophilic membrane marker rhodamine-B-phosphoethanolamine (Rh-PE) and incubated with COS-7 cells. Further, the cells were stained with specific markers: the cell membrane was fluorescently labeled with Vybrant DiO, lysosomes were stained with LysoTracker Red, and 4',6 diamidino-2-phenylindole dihydrochloride was used for counterstaining the nucleus.

Results: All five dyes were used simultaneously and were spectrally distinguished by the system. FITC-dextran-la-

beled liposomes showed a distribution pattern different from identically composed liposomes labeled with Rh-PE: the highly lipophilic Rh-PE was colocalized with the lysosomotropic dye LysoTracker Red, whereas liposomal FITC-dextran was not accompanied by LysoTracker Red in all cases.

Conclusions: (a) Spectral (bio-) imaging is a powerful method for studying the intracellular fate of liposomal compounds. (b) We assume that the liposome membrane marker Rh-PE influences the uptake of particles due to its surface-modifying properties. We propose that this head-group-labeled phospholipid acts as a ligand for cellular receptors and triggers receptor-mediated (clathrin-dependent) endocytosis. *Cytometry Part A 57A:10–21, 2004.*

© 2003 Wiley-Liss, Inc.

Key terms: pH-sensitive liposomes; COS-7 cells; spectral bio-imaging; multicolor imaging; Fourier spectroscopy; intracellular trafficking; Rh-PE

Liposomes are widely used as drug delivery systems to transfer macromolecules or other substances to target cells (1–3). To improve the efficiency of the drug targeting, it is necessary to understand the mechanism of liposome uptake by the cell and to follow the intracellular fate of internalized liposomes and their contents (4).

Even though cell biologists have been studying the cellular uptake of particles by fusion or endocytosis for almost one century, the mechanism of uptake and intracellular trafficking of liposomes is still poorly understood.

Endocytosis is described as a diverse set of processes used by the cell to internalize specialized regions of the plasma membrane and small amounts of extracellular fluid. In 1964 Roth and Porter identified clathrin-coated pits as particular plasma membrane domains responsible for the selective recruitment of cargo molecules (5). Other types of endocytosis (6,7) include those mediated by caveolae, small flask-shaped vesicles rich in cholesterol and signaling molecules, and so-called clathrin-independent pathways that involve neither clathrin-coated pits nor caveolae. In addition, some cell types are capable of internalizing large amounts of fluid via macropinocytosis or large particulates by phagocytosis.

The type of endocytosis, which is best understood, is the clathrin-dependent uptake that transports endocytosed material via early endosomes, carrier vesicles, and late endosomes to digesting lysosomes that contain a broad spectrum of peptidases and hydrolases in an acidic surrounding. If material reaches the lysosomes, it might be digested and inactivated. Therefore, liposomes, or at least their active contents, should escape from the endosomal system into the cytoplasm before this degradation happens. One strategy is the concept of pH-sensitive liposomes that are designed to fuse with the endosomal membrane, releasing their contents directly into the cytoplasm, or become destabilized and subsequently destabilize the

Ulrich Huth and Ansgar Wieschollek contributed equally to this publication.

*Correspondence to: Ulrich Huth, Department of Pharmaceutical Technology, Albert-Ludwigs University, Stefan-Meier-Str. 19, D-79104 Freiburg, Germany.

E-mail: ulrich.huth@pharmazie.uni-freiburg.de

Published online in Wiley InterScience (www.interscience.wiley.com). DOI: 10.1002/cyto.a.10105

endosomal membrane, resulting in leakage of the endosomal contents into the cytosol (8).

In the broad field of liposome research, fluorescent methods are used to follow the cellular association of liposomes (9–11) and the intracellular trafficking of endocytosed material (12,13).

Methods dealing with fluorescent dyes include the immunofluorescent staining of cells and tissues and the staining of different cell organelles such as lysosomes, mitochondria, and the nucleus (14–16).

Many different fluorophores are currently available with emission spectra that cover the entire visible-light and near-infrared spectrum. The spectral shift of the emission spectrum toward longer wavelengths compared with its absorption spectrum (also called the Stokes shift) makes it possible to separate excitation light from emission light by performing fluorescence spectroscopy or by using optical filters in microscopy (17). Fluorescent microscopy measurements are based mostly on epifluorescence. Because the emission intensity is usually a few orders of magnitude lower than the excitation intensity, it is necessary to block the excitation light from the emission path. This is done by using a set of filters (usually three) in the light path of the microscope.

In multicolor measurements, several fluorophores are used simultaneously. To distinguish between the emission lights from these dyes, the lights should have a negligible degree of spectral overlap. In addition, other requirements for the fluorophores such as high brightness and stability have to be fulfilled.

Fluorescent dyes can be used in different analytical methods: fluorescence-activated cell sorting analysis (FACS) (or flow cytometry) provides quantitative information and is particularly useful for the detection of fluorescently labeled cells (18). However, with this method, it is not possible to distinguish between material that is attached to the cell membrane and material that is taken up by the cell. Further, the number of dyes that can be used simultaneously is limited. Fluorescence microscopic techniques provide spatial information of the sample of interest (9,19) but provide only limited information about the spectral features of the sample.

The problem of measuring several dyes simultaneously and distinguishing them on a quantitative basis was significantly improved in recent years by novel optical methods and setups, mainly for applications in the field of molecular cytogenetics. These methods include spectral karyotyping (20), multiplex fluorescence in situ hybridization (M-FISH) (21), COBRA-FISH (22), and others, which are based on a particular method to distinguish the different fluorochromes. This can be achieved by using sets of filters that are designed to have optimal spectral ranges for the excitation and emission bands of the set of fluorochromes or by measuring the complete spectrum for each point of the image.

In the presented study, a spectral imaging technology was applied. Spectral imaging is especially useful for the examination of multifluorescent samples. By combining spectroscopy and imaging, this method enables the simul-

taneous measurement of the fluorescence spectrum for each pixel of the microscopical image (20,23,24) without changing the filter set. For this purpose, a triple bandpass filter set was used. Subsequent analysis of the measured data results in the exact localization of each dye in the image.

An inverted fluorescence microscope equipped with a high-pressure mercury lamp for excitation was used. The optical head attached to the microscope is composed of a Sagnac common-path interferometer (25) and imaging optics including a cooled CCD camera.

The light emitted by the fluorophores in the sample enters the interferometer, is split into two coherent beams that travel in opposite directions, and creates an optical path difference (OPD). The OPD can be changed by tilting the mirrors of the interferometer in a small angle. At the exit, the two beams are recombined to interfere with each other, and the CCD camera measures the resulting interference intensity as a function of the OPD. During a measurement, the intensity versus OPD function (called the interferogram) is collected simultaneously from each of the 659×496 pixels of the CCD array, which is then Fourier transformed, a process that enables the recovery of the spectrum of the light (26). The extracted spectral image can be displayed in human vision colors or analyzed further to identify the quantitative contents of different dyes.

To categorize the applied spectral bio-imaging method, the basic types of spectral dispersion methods that might be considered for a spectral bio-imaging system are briefly summarized: (a) grating and/or prism, (b) bandpass filters, and (c) interferometric spectroscopy. Other recently developed methods are computed tomographic imaging spectroscopy (CITS) and confocal-based spectral imaging.

In grating/prism (i.e., monochromator)-based systems, also known as slit-type imaging spectrometers, the field of view is limited at any given time to a line of pixels. Therefore, a full image can be obtained only after scanning the grating or the incoming beam in a direction parallel to the spectral axis of the CCD (line scanning). Slit-type imaging spectrometers also have a major disadvantage because most of the pixels of one frame are not measured at any given time. The efficiency of the measurement is therefore reduced.

Filter-based spectral dispersion methods can be further categorized into discrete filters and tunable filters. Similar to the slit-type imaging spectrometers equipped with a grating, most of the radiation is rejected at any given time. Tunable filters, such as acousto-optic tunable filters (AOTF) (27) and liquid-crystal tunable filters (LCTF) (28), have no moving parts and can be tuned to any particular wavelength in the spectral range of the device in which they are implemented. Interferometer-based systems work on the same principle as Fourier transform spectrometers. In a spectral imaging system, the interferometer is positioned in a real imaging-optics system that ensures that changes of the optical path difference inside the interferometer do not create any shift of the image on the CCD. In such systems, there is no need to use narrow filters or

slits to measure the spectral image. The efficiency of the measurement in principle therefore is high due to the collection efficiency. Roughly speaking, all the wavelengths are measured for the whole image with an average efficiency of 0.5 because of the modulation; therefore, this method is advantageous over the other methods.

CITS is a non-scanning instrument that simultaneously acquires a full spectral image during a single integration time. The spectral and spatial resolutions of such a system in principle are high enough for the analysis of physiologic responses within living biological specimens (29). The method definitely has an advantage for *in vivo* measurements when short measurement times are required, but the practical potential of the method remains to be explored.

Another recently developed method is based on a confocal scanning laser that measures the image point by point. In this method, the detected light passes through a spectrometer and the spectral image is constructed (23). This system in general is more complex and also allows three-dimensional reconstruction of the images and lifetime measurements.

In other microscopic systems such as conventional fluorescence microscopy or confocal microscopy, only a limited number of fluorescent dyes can be used in one measurement. Further, the acceptable level of overlapping of the excitation and emission spectra of these dyes is limited and requires a unique filter set for every single dye that also depends on the set of other dyes being used. The use of conventional microscopes with specially designed filters has been described by Farkas et al. (24) and Eils et al. (30).

In the present study it is demonstrated that the use of the spectral imager eliminates most of the limitations of simultaneous detection of fluorescent markers in a single measurement, which makes it possible to distinguish between stained liposomal membranes, liposomal content, and several cell organelles by using five dyes at the same time. Similar measurements have been performed with up to seven dyes in studies of cellular antibody distribution (31). However, they used three different (long pass) filters with a special isolation of only three dyes at each time.

In our experiments, we followed the uptake and intracellular fate of liposomes and their contents, and we used five fluorescent dyes in one sample. Spectral bio-imaging enabled the detection and separation of several, even spectrally overlapping, dyes in one measurement. We concluded that spectral bio-imaging is a method that best meets our requirements for studying the intracellular trafficking of liposomes.

MATERIALS AND METHODS

Materials

LysoTracker Red, rhodamine-B plus phycoerythrin (Rh-PE; lissamine; rhodamine-B: 1,2-dihexadecanoyl-sn-glycero-3-phosphoethanolamine), Vybrant DiO cell-labeling solution, and 4',6 diamidino-2-phenylindole dihydrochloride (DAPI) were purchased from Molecular Probes (Lei-

den, The Netherlands). Cholesteryl hemisuccinate morpholine salt (CHEMS) and fluorescein isothiocyanate-dextran (FITC-dextran; molecular weight 4,400) were purchased from Sigma (Deisenhofen, Germany). Dioleoyl phosphatidylethanolamine (DOPE) was a generous gift from Lipoid (Ludwigshafen, Germany). All other chemicals were of analytical grade.

Liposome Preparation

Liposomes were prepared by using freeze-thaw cycles and the extrusion method (32,33). The pH-sensitive liposomes were composed of DOPE:CHEMS in a molar ratio of 3:2. The lipids and, optionally, the lipophilic marker Rh-PE (0.5 mol%) were dissolved in ethanol:chloroform (3:1 vol/vol) in a 50-ml round-bottom flask. The solvent was removed by rotary evaporation and vacuum desiccation for 1 h. The dry lipid film was hydrated to yield a final concentration of 50 mmol of lipid per liter by the addition of 1 ml HEPES buffer (10 mM HEPES, 150 mM NaCl, pH 7.4) optionally containing the hydrophilic marker FITC-dextran (10 mM). The liposome dispersion was rapidly frozen in liquid nitrogen and thawed for 20 min at room temperature three times. The resulting multilamellar vesicles were extruded 27 times with a LipoFast extruder (Avestin, Ottawa, Canada) through a polycarbonate filter with 200-nm pore size (Nuclepore, Pleasanton, USA). The lipid concentration was determined by using a phosphorus assay (34), and the liposome size was measured by photon correlation spectroscopy using a Nicomp 380 ZLS (Santa Barbara, CA). The diameter of the vesicles was in the range of 180 to 220 nm.

Before incubation, nonencapsulated FITC-dextran was removed by gel permeation chromatography on a Sepharose CL-4B (Pharmacia, Upsala, Sweden) column measuring 0.7×20 cm (Biorad, München, Germany). The separated liposome fraction with encapsulated FITC-dextran and the fraction with free marker (FITC-dextran) were measured fluorometrically (LS-50 B, Perkin Elmer, Überlingen, Germany) at $\lambda_{\text{exc}} = 493$ nm and $\lambda_{\text{em}} = 514$ nm in the presence of 20 mM sodium cholate. The encapsulation efficiency was approximately 15%. Single-labeled liposomes were prepared to contain the hydrophilic dye FITC-dextran or the lipophilic marker Rh-PE.

Cell Culture and Incubation With Liposomes

COS-7 cells (monkey kidney, simian virus 40 transformed) were routinely grown as monolayers in 100-mm Falcon tissue culture dishes. Cells were kept in a humidified 5% CO₂ atmosphere at 37°C. They were cultured in Dulbecco's modified Eagle's medium without phenol red and supplemented with 10% fetal calf serum, 1% L-glutamine (---) 200 mM (Biochrom, Germany), and 1.8 g/l glucose. For microscopic examinations, cells were seeded onto 12-mm coverslips in 24-well plates (Falcon, Germany) 2 days before use. Before the experiment, cells were washed twice with 1 ml of phosphate buffered saline (PBS) and then incubated for 1 h with 300 μ l of Dulbecco's modified Eagle's medium (without fetal calf serum) containing liposomes (1 mM total lipid concentra-

tion) loaded with FITC-dextran or Rh-PE. After incubation, cells were washed twice with 1 ml of PBS.

Cell Marker

In case LysoTracker Red was used, the dye was added to cells and liposomes 30 min after starting the incubation. The dye was used at a concentration of 0.5 μM for staining acidic cell organelles such as endosomes and lysosomes. At the end of the 1-h liposomal incubation time (30 min for LysoTracker and 30 min for cells), the cells were washed twice with 1 ml of PBS (without $\text{Ca}^{2+}/\text{Mg}^{2+}$). Subsequently, 100 μl of DiO staining medium (1 μM) was added onto the corner of the coverslips for cell membrane staining. The plates were agitated gently until all cells were covered with staining medium. After 15 min of incubation at 37°C in 5% CO_2 , the coverslips were washed three times with PBS (without $\text{Ca}^{2+}/\text{Mg}^{2+}$). Cells were fixed with 4% paraformaldehyde (500 μl , 10 min, room temperature) and washed again twice with 1 ml of PBS (without $\text{Ca}^{2+}/\text{Mg}^{2+}$). DAPI was added to the wells (300 μl , 0.1 μM , 20 min, room temperature) for counterstaining the nucleus in blue. Cells were washed five times with 1 ml of PBS (without $\text{Ca}^{2+}/\text{Mg}^{2+}$). For fluorescence imaging, the coverslips were mounted on glass slides with 4 μl of Vectashield (Linaris, Wertheim-Bettingen, Germany), an antifading substance, to reduce photobleaching effects (35). To fix the coverslips on the slides, nail polish was applied to the edges.

Spectral Bio-Imaging

Spectral imaging was performed with a SpectraCube SD-200H system (Applied Spectral Imaging, Migdal HaEmek, Israel). The system enables the measurement of spectral information from each pixel of an observed image (25,36). We used an inverted fluorescence microscope (Axiovert S 100, Zeiss, Jena, Germany) equipped with a high-pressure mercury lamp (HBO 100) for excitation and a triple bandpass filter set (see below). All images were taken with a 40 \times /1.3 oil-immersion objective lens (Plan Neofluar, Zeiss). In the spectral range from 400 to 700 nm, the objective lens shows only minimal fluctuations of transmission (85–90%). The optical head attached to the microscope is composed of a Sagnac common-path interferometer (25) and imaging optics including a cooled CCD camera (C4880-85, Hamamatsu, Japan).

The best achievable spectral resolutions are 5 nm at 400-nm wavelength and 12 nm at 600-nm wavelength (the spectral resolution of a Fourier-based spectrometer is constant in the energy or wavenumber domain), and the spectral range is 400 to 1000 nm (37). The spectral resolution is limited by the largest possible rotation of the interferometer before vignetting occurs. The spectral resolution for the measurement can easily be varied before each acquisition by setting the required parameter in the acquisition program. This parameter determines the required maximal OPD for the provided acquisition (i.e., the maximal rotation angle for the interferometer). This is an important advantage that can help to optimize each series of measurements.

Table 1
Spectral Characteristics of the Filter Set

Filter set	Exciter ^a	Dichroic mirror	Emitter ^a
Triple bandpass filter	392F8	407	458F9
	484F8	497	520F15
	557F12	572	602F21

^a“F” means full band width at 50% transmission; filters are named after their center wavelengths; the 392F8 filter transmits light from 384 to 400 nm.

Spectral shifts along the image are low and are measured to be less than 1 nm from the central pixel to pixels at the edge of the CCD.

The intensity uniformity of the image is high and is basically limited by the nonuniformity of the microscope light excitation. Typically, a change of uniformity of less than 15% along the image is measured.

The cooled 12-bit CCD has a low dark and readout noise and allows measurements up to 20 s before dark noise becomes significant. The pixel size of the CCD is 10 \times 10 μm . The spatial resolution of the system is basically diffraction limited by the microscope numeric aperture, magnification, and pixel size; with a 40 \times objective lens, the spatial resolution is 0.25 $\mu\text{m}/\text{pixel}$. The CCD is an interline CCD with microlenses that provides high collection efficiency (>85%). The spectral response of the CCD peak is 75% at about 550 nm. The camera has a frame-transfer time of 80 ms and therefore allows the measurement of a stack of images continuously. The total acquisition time depends on the number of OPDs that is selected (typically 128) multiplied by the exposure time per frame.

Fluorescence Filter Set

A triple bandpass filter set (Chroma, AHF, Tübingen, Germany) was used for simultaneous detection of blue, green, and red fluorescent dyes, e.g., DAPI/FITC/Rh-PE/LysoTracker Red/Vybrant DiO. The spectral characteristics are shown in Table 1.

Spectral Analysis

Microscopic images were obtained with Spectral Imaging 2.5 software (Applied Spectral Imaging). The acquisition time of a desired image varied from 30 to 90 s depending on the brightness of fluorescence and the image size. First cells were incubated with only one dye to get single-colored images. For further analysis, images were transferred to the SpectraView 1.6 software (Applied Spectral Imaging). A global background subtraction algorithm was applied to improve the signal-to-noise ratio. This algorithm automatically (or manually) detects the background spectrum and its intensity variations along the image. The amount of background subtracted corresponds to its intensity in the region. The result is a uniform spectral image for which the spectra represent the pure color of the dyes without any autofluorescence or leakage of excitation light. By setting a marker on a de-

sired pixel, the fluorescence emission spectra were defined and stored in the library as reference spectra.

Spectral Unmixing (SUN) Algorithm

The SUN algorithm separates multicolor images into its fluorescent components by comparing the reference spectra from the library with the emission spectra that were measured for each pixel in the image. As a result, the intensity of each dye is extracted at each pixel and provides information on the localization of each dye in the image. The SUN algorithm takes as an input the spectral image $S_{x,y}(\lambda)$, where x,y describes the pixel coordinates and the set of N reference spectra (the number of dyes used), $I_i(\lambda)$, $i = 1, 2, \dots, N$, and calculates a set of N values for each pixel that reflects the contribution of each dye.

Each one of the many measured spectra, $S(\lambda)$, can be described as a linear combination of the N known fluorescence reference spectra, $I_i(\lambda)$; $i = 1, 2, \dots, N$, i.e., $S(\lambda) =$

$$\sum_{i=1}^N c_i \cdot I_i(\lambda). \text{ The set of coefficients } c_i \text{ can be de-}$$

scribed as a vector $C = (c_1, c_2, \dots, c_N)$ that solves the following matrix equation:

$$\begin{bmatrix} S(\lambda_1) \\ S(\lambda_2) \\ \vdots \\ S(\lambda_M) \end{bmatrix} = \begin{bmatrix} I_1(\lambda_1) & I_2(\lambda_1) & \dots & I_N(\lambda_1) \\ I_1(\lambda_2) & I_2(\lambda_2) & & \\ \vdots & \vdots & \ddots & \\ I_1(\lambda_M) & \dots & & I_N(\lambda_M) \end{bmatrix} \times \begin{bmatrix} c_1 \\ c_2 \\ \vdots \\ c_N \end{bmatrix} = \bar{F} \times \begin{bmatrix} c_1 \\ c_2 \\ \vdots \\ c_N \end{bmatrix}$$

where each spectrum consists of M points, i.e., $\lambda_1, \lambda_2, \dots, \lambda_M$ and the matrix above is defined as \bar{F} . In general in our study, the number of equations in the matrix was larger than the number of coefficients ($M > N$), and the matrix is therefore overdetermined. In general, there will not be an exact solution to the problem due to another sort of fluorescence that is not related to the dyes themselves and due to different sorts of noise (26), and therefore the best compromise is calculated. The difference between the solution that is found and the actual measured spectrum can be compared, and the validity of the solution can be determined based on this. If the best solution is defined by means of least squares, i.e., that the sum of squares of the differences between the left- and right-hand sides of the matrix equation above is minimized, then the problem is reduced to a usually solvable linear least-square problem. The reduced set of equations to be solved can be written as:

$$(\bar{F}^T \cdot \bar{F})C = \bar{F}^T \cdot S$$

where C is the unknown row vector of coefficients, S is the row vector of the spectrum being decomposed, and \bar{F}^T

stands for the transposed matrix. Finding the inverse matrix $(\bar{F}^T \cdot \bar{F})^{-1}$ can easily solve this equation.

The algorithm that is used here is similar to the one that is being used for spectral karyotyping. This algorithm has been widely tested and used, and many findings have been made, verified, and published. See, for example, a review on hundreds of cases by Schröck et al. (38).

Once the set of coefficients C is found for each pixel, there are different possible calculations that can be based on it and different display methods. As an example, it is possible to create N different images that reflect the contribution of a single dye to the image. Each image can be displayed in a selected color that is not necessarily similar to the original color of the dye.

Even though the optical setups are different, spectral karyotyping, M-FISH, COBRA-FISH, and other methods share the same principle that enables them to acquire data that can be analyzed so that dyes that are spectrally overlapping can still be unmixed and analyzed. The problem of unmixing spectrally overlapping dyes was broadly discussed before (26,39) and will not be repeated here. In these papers, it is concluded that the problem is solved by all these methods with various advantages and disadvantages to each one method, an issue that is beyond the scope of this paper.

The method based on Fourier transformation resolves the problem overlapping dyes by measuring spectral images with high spatial and spectral resolutions. The spectrum that is measured at each pixel enables differentiation of dyes that have a spectral difference of their maxima as low as 10 nm. An adequate filter cube has to be used that allows the simultaneous excitation and detection of all these dyes.

RESULTS

We successfully used a triple bandpass filter set that consists of an excitation filter with wavelength windows for simultaneous excitation of blue, green, and red fluorescences, a triple dichroic mirror, and a triple bandpass emission filter (Fig. 1). The exact spectral data of the triple bandpass filter are shown in Table 1. The three filters are combined in a filter cube, and a good rejection ratio is achieved (in the range of 10^{-4} to 10^{-7} , which is high enough for high-quality fluorescence measurements). With this filter cube, all dyes are efficiently excited simultaneously without having to change any filters during the measurement. The emission spectra obtained with the triple bandpass filter set and the SpectraCube (Fig. 2A) differ from the emission spectra acquired with a fluorescence spectrometer (Fig. 2B). The difference is due to the convolution of the real spectrum with the filters and the system response (CCD, optics, etc.). The spectra shown in Figure 2A were taken from single-colored images, as described below, and were used to create the spectral library. They are reloaded from this library as reference spectra for the spectral analysis of multicolor images, and the same acquisition parameters (such as the spectral resolution) are used for all the measurements.

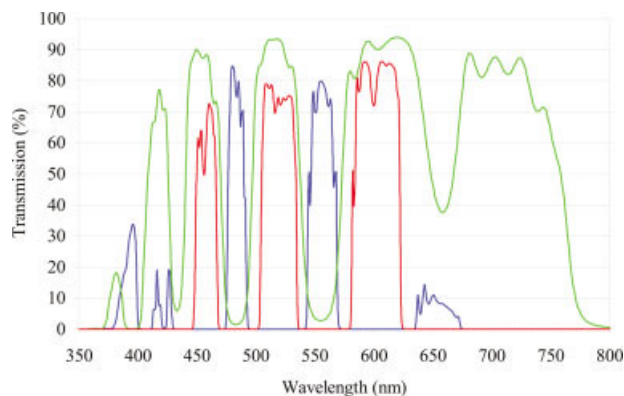


FIG. 1. Spectral data of the triple bandpass filter. Transmission spectrum of excitation filter (blue), transmission spectrum of emission filter (red), and spectrum of dichroic mirror (green).

To overcome a noticeable bleaching effect (particularly of FITC-dextran), we embedded the cells in an antifading mounting medium, and the fluorescence remained stable during the acquisition time. All staining experiments, including the single-colored images, were performed with this mounting medium because the antifading substance causes spectral shifts of the dyes.

Single-Color Images to Create the Library

To create the spectral library, which is the basis for the SUN algorithm, single-color experiments were performed (Fig. 3). All images were acquired by using the filter described above. The intensity at each pixel reflects the brightness of the dye, as calculated by the spectral intensity. Figure 3A shows the result of incubation of the cells with pH-sensitive liposomes containing FITC-dextran. Cell membrane and cytoplasm show strong green fluorescence, indicating that liposomes are bound to the cell surface and are taken up by the cell. The fluorescence can be seen diffusely throughout the cytoplasm of the cell and also in vesicular structures of the cell. Liposomal-incorporated Rh-PE (Fig. 3B), a commonly used fluorophore in liposome research, appears as punctuated in the cytoplasm and in the perinuclear area. LysoTracker Red is a red fluorescent acid-tropic dye that accumulates in acidic organelles of living cells. It diffuses freely through cell membranes. In acidic organelles, the dye as a weak base is protonated and captured in the membranes of these organelles. The staining includes endosomes and lysosomes (40). Figure 3C shows that most of the dye is indeed concentrated in the peripheral and central vesicular compartments of the cell. When using LysoTracker Red with fixed cells, a higher concentration of the dye is required to compensate for the loss of fluorescence after fixation. Counterstaining the nucleus with DAPI resulted in a very bright and dominant fluorescence (Fig. 3E). It was necessary to reduce the concentration of this dye to a minimum to prevent superimposing effects of adjacent fluorophores. The fifth fluorescent dye used was Vybrant DiO, a lipophilic and low-cytotoxic carbocyanine dye (41). In

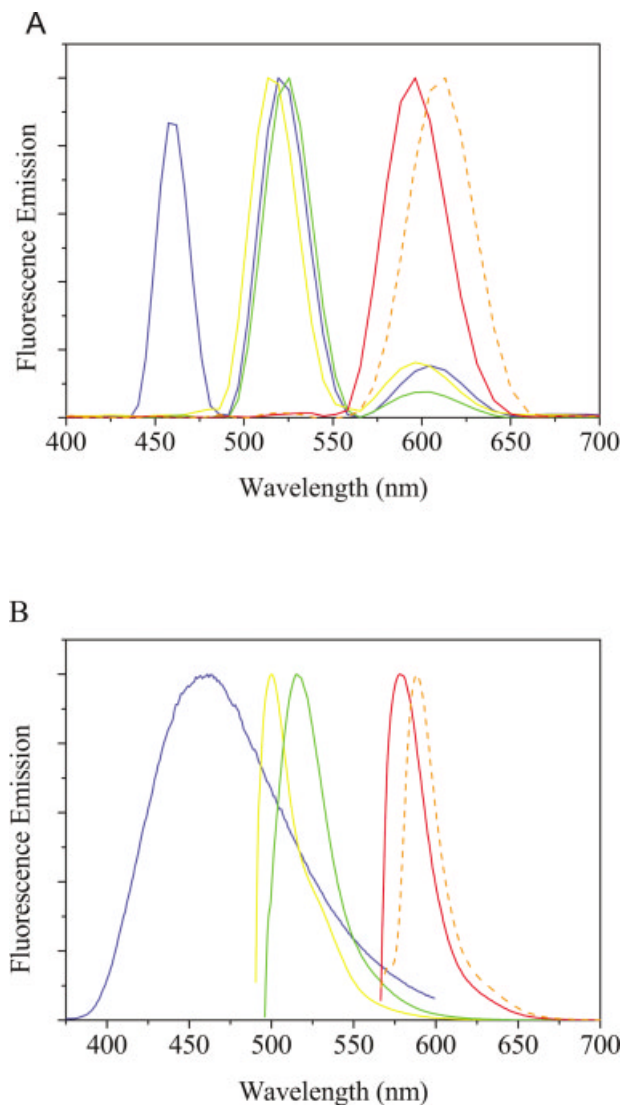


FIG. 2. Fluorescence emission spectra of dyes: DAPI (blue), Vybrant DiO (yellow), FITC-dextran (green), Rh-PE (red), and LysoTracker Red (orange dotted lines). **A:** Spectra measured with the triple bandpass filter set in presence of cells and the antifade reagent. **B:** Spectra from the literature (Molecular Probes, Leiden, The Netherlands) measured with a fluorescence spectrometer: DAPI bound to DNA, Vybrant DiO (in methanol), FITC-dextran (in HEPES buffer, pH 7.4), Rh-PE (in methanol), and LysoTracker Red (in methanol).

addition to the fluorescent plasma membrane, intracellular membrane structures were stained (Fig. 3D). Detailed information about spectral data of the dyes is presented in Table 2.

Two- and Three-Color Images to Demonstrate the System's Suitability

After creating the spectral library from single-stained images, experiments with multicolor samples were performed. In the first series, two red dyes with a wide spectral overlap were applied (Fig. 4A). The second series shows two green fluorescent dyes in combination with a

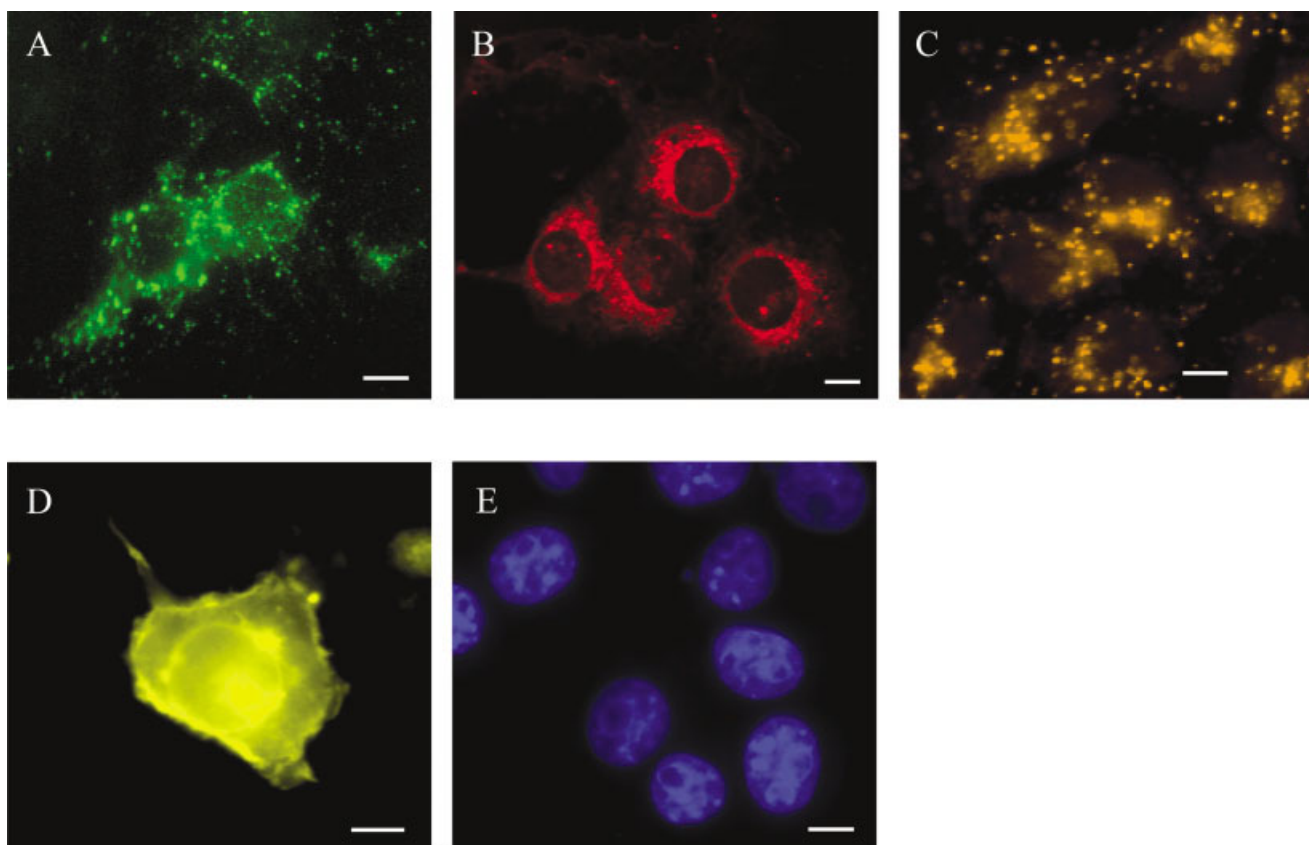


FIG. 3. Single-stained COS-7 cells. Pixels represent localizations of the dyes in false colors, which were assigned to the reference spectra by the operator. Cells were incubated with pH-sensitive liposomes (1 mM final lipid concentration) containing (A) FITC-dextran or (B) Rh-PE in RPMI medium without fetal calf serum (1 h, 37°C, 5% CO₂). C: Acidic compartments stained with LysoTracker Red (0.5 μM, 30 min). D: Membrane of the cells stained with Vybrant DiO (100 μl of staining medium, 1 μM, 15 min). E: Blue counterstaining of the nucleus with DAPI (0.1 μM, 20 min). All images were obtained with the triple bandpass filter set. Scale bars = 10 μm.

blue fluorescent dye. It should be noted that the emission maxima only differ in 10 nm for the red and 12 nm for the green dyes (Table 2 and Fig. 2A), which is below the human resolution limit. The SpectraCube system's technical and theoretical limitations in the longer wavelength region occur as a spectral resolution of 10 nm in difference (as for LysoTracker Red and Rh-PE).

The result of double-colored COS-7 cells (red dyes) is shown in Figure 4A (I-III). After background subtraction, the fluorescence SUN algorithm was applied to the original image (Fig. 4AD) by using the reference spectra. The

Table 2
Spectral Characteristics of the Used Dyes

Dye	Maximum excitation (nm)	Maximum emission (nm)
DAPI	358	461
Vybrant DiO	484	501
FITC-dextran	493	514
Lissamine Rh-PE	555	580
LysoTracker Red	577	590

single-color SUN images (Fig. 4AI,II) present the localization of the labels displayed in false colors.

The LysoTracker Red is located predominantly in the perinuclear area, as expected for late endosomes and lysosomes. The liposomal membrane label Rh-PE is found close to the plasma membrane but is also colocalized with LysoTracker Red in acid compartments near the plasma membrane after 1 h of incubation.

Further multicolor experiments were performed with three spectrally overlapping dyes (Fig. 4BI-IV). Two green fluorescent dyes (FITC-dextran and Vybrant DiO) and DAPI with a blue fluorescence were used. The published emission maxima (Table 2) of DiO and FITC-dextran differ for 12 nm and is reduced to 6 nm (DiO $Em_{max} = 519$ nm; FITC-dextran $Em_{max} = 525$ nm) when using the triple bandpass filter. The broad spectrum of DAPI resulted in an extensive fluorescence in the green emission window of the filter, almost matching the DiO emission spectrum. The system enables the simultaneous detection and spectral resolution of these highly spectrally overlapping dyes. Further, the localization of the dyes in the cell is plausible. Most FITC-dextran

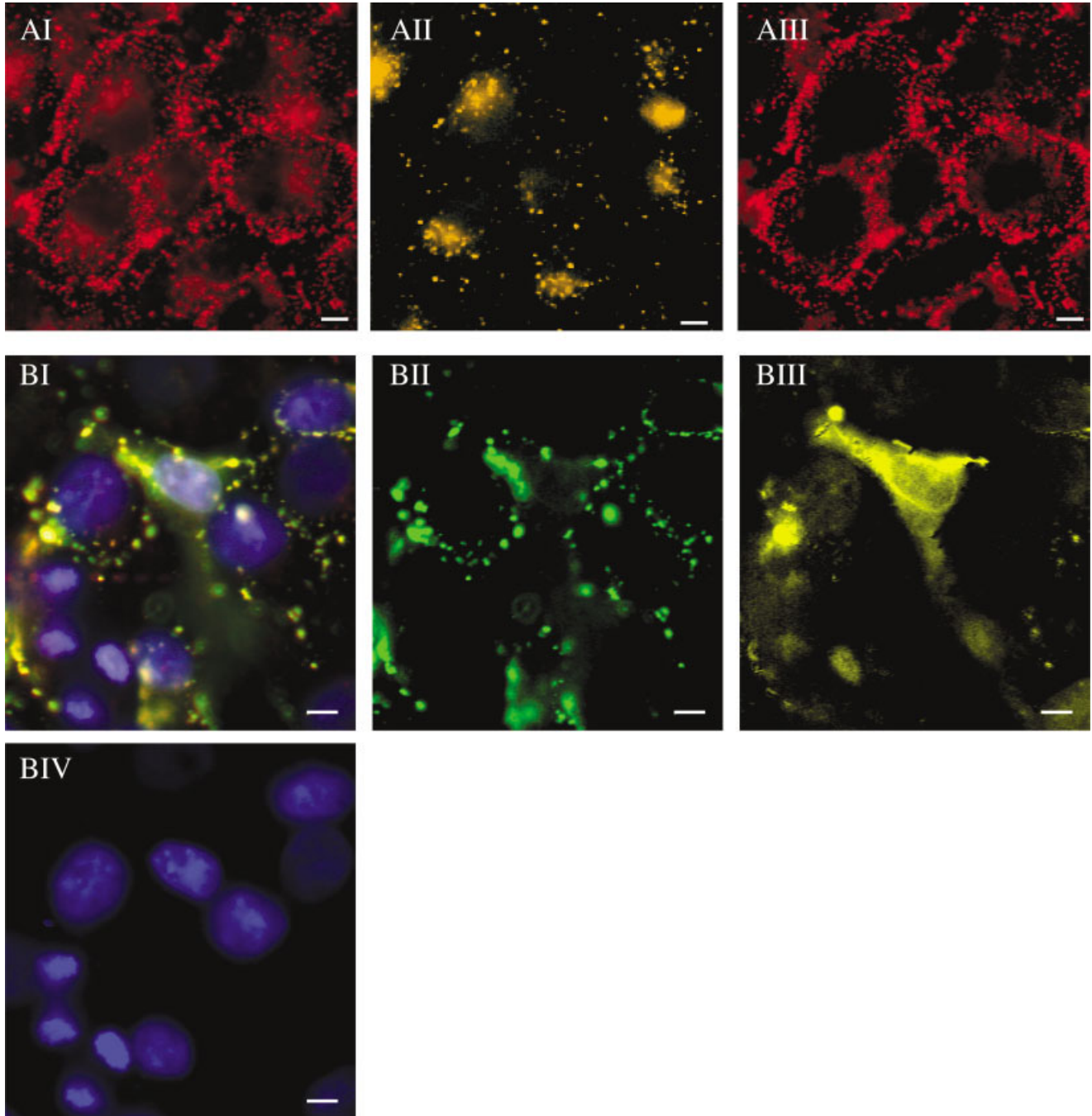


FIG. 4. **A:** Double-stained cells. Incubation of COS-7 cells with pH-sensitive liposomes labeled with Rh-PE and staining of acidic organelles with LysoTracker Red. I: Original view. Pictures were taken with Spectral Imaging 2.5 software. After applying the SUN algorithm, pixels with the spectrum of Rh-PE are colored in red; pixels with the spectrum of LysoTracker Red are colored in orange. The exact localizations of (II) LysoTracker Red and (III) Rh-PE are shown. **B:** Triple-stained cells. Incubation of COS-7 cells with pH-sensitive liposomes containing encapsulated FITC-dextran. Additional staining of the cell membrane with Vybrant DiO and of the nucleus with DAPI. I: Original view after image acquisition. The exact localizations of (II) FITC-dextran, (III) Vybrant DiO, and (IV) DAPI are shown. Images were obtained with the triple bandpass filter set. Scale bars = 10 μm .

signals were located in vesicles near the cell membrane (Fig. 4BII). DiO membrane staining turned out to be efficient only in one cell of the image (Fig. 4BIII), for unknown reasons. The DAPI staining of the nucleus was successful in all cells (Fig. 4BIV).

Intracellular Trafficking of pH-Sensitive Liposomes Analyzed With Multicolor Images

On the basis of these results, several multicolor studies with five dyes were performed. The images (Fig.

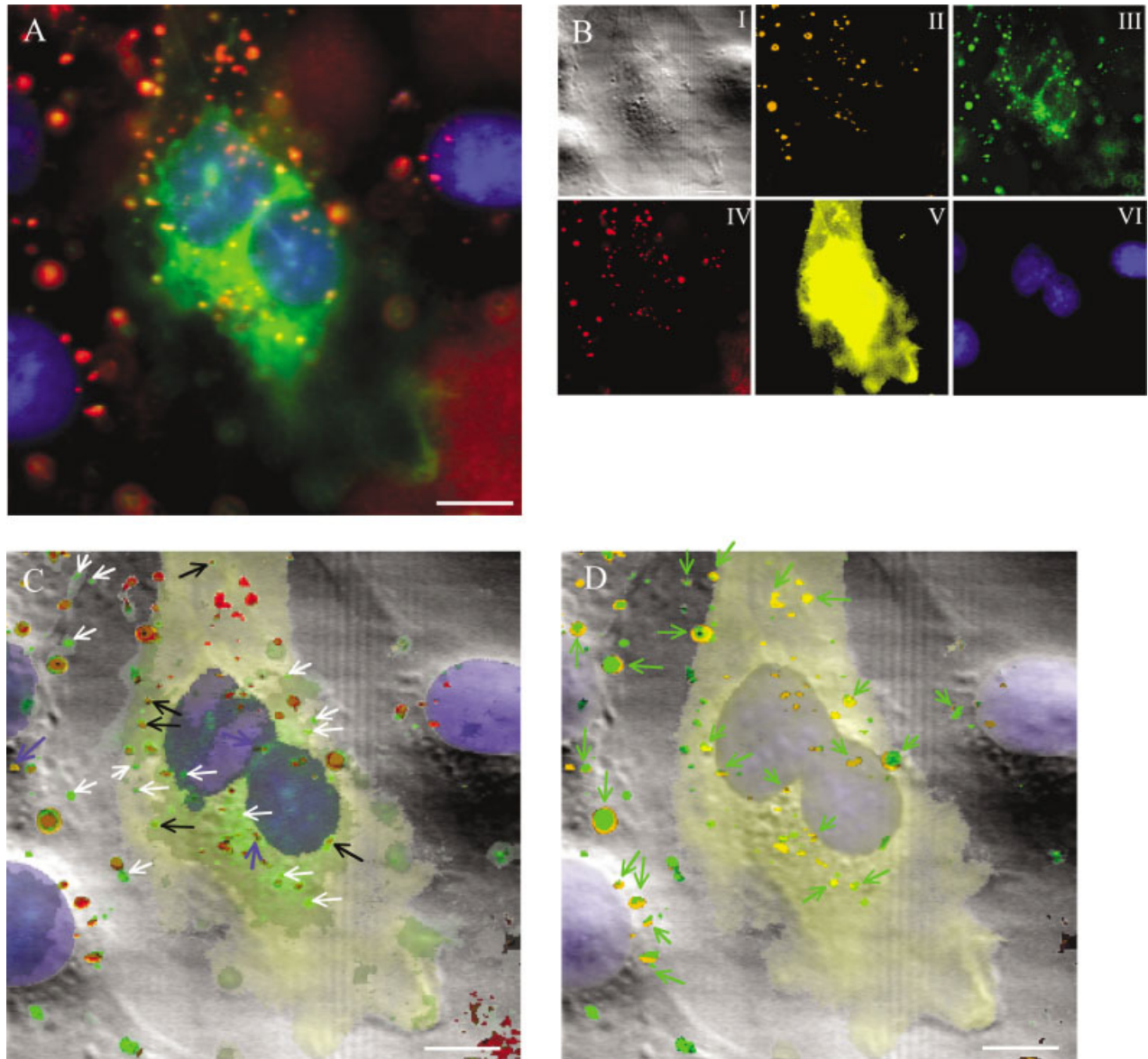


FIG. 5. Multicolor study with five dyes and COS-7 cells: (A) original view, (B) brightfield image of the same group of cells, (BII–VI) spectrally decomposed single-color images: (II) LysoTracker Red, (III) FITC-dextran, (IV) Rh-PE, (V) Vybrant DiO, and (VI) DAPI. C: Overlay of the brightfield image and the five spectrally decomposed single-color images. In the image the colors of DiO and DAPI are reduced to give an orientation in the cell but not to draw conclusions from the intensity. Black arrows indicate the positions of Rh-PE that are not accompanied by the staining of LysoTracker Red. White arrows indicate FITC-dextran that is accompanied by neither Rh-PE nor LysoTracker Red. Only a few spots are stained exclusively with LysoTracker Red (blue arrows). D: Overlay of the brightfield image and single-color images of FITC-dextran and LysoTracker Red. DAPI and DiO are displayed in reduced colors. Green arrows point to FITC-dextran vesicles that are located in acidic compartments stained with LysoTracker Red. Scale bars = 10 μm .

5A–D) show a group of COS-7 cells growing in monolayers, thus representing normal growth conditions. Cells were incubated for 30 min with liposome preparations containing FITC-dextran or Rh-PE and then with LysoTracker Red for another 30 min followed by cell membrane staining with DiO for 15 min. After fixation of the cells, the nuclei were counterstained with DAPI. The results of this quintuple image represent a vesicle distribution typical for this experimental setup (Fig. 5). The original view in shown in Figure 5A presents the

image in the fluorescence microscope, and image Figure 5BI shows the cells viewed through the brightfield microscope.

The different spectrally resolved single-color images (Fig. 5BII–VI) were analyzed with a powerful imaging software (SpectraView, Applied Spectral Imaging; Adobe Photoshop 6.0, Adobe Systems, USA) for colocalization of the dyes. Figure 5C is a combination of the brightfield image and the five single-color images. The intensities of the colors were chosen arbitrarily. Therefore, no conclu-

Table 3
*Statistical Summarization of Vesicle Distribution**

	Relative distribution	Deviation
Distribution of FITC-dextran ^a (liposomes)		
FITC-dextran colocalized with LysoTracker Red	52%	11.2%
FITC-dextran not in colocalization with LysoTracker Red	48%	
Distribution of Rh-PE (liposomes)		
Rh-PE colocalized with LysoTracker Red	73%	8.4%
Rh-PE not in colocalization with LysoTracker Red	27%	
Distribution of Rh-PE + FITC-dextran ^a (liposomes)		
Rh-PE colocalized with FITC-dextran	81%	<10%
Rh-PE not in colocalization with FITC-dextran	19%	
FITC-dextran colocalized with Rh-PE	70%	<10%
FITC-dextran not in colocalization with Rh-PE	30%	

*The vesicle distribution of five independent experiments with a total number of about 1,000 vesicles in 15 well-stained cells was analyzed.

^aDistribution of vesicular FITC-dextran (no attention to diffuse fluorescence).

sions concerning quantities of the dyes can be drawn from this display. Despite the transparent display of the dyes, colocalization of the different colors can only be seen clearly only in distinct spots. However, by analyzing the spectra in each pixel, the presence and quantity of each single dye can be determined.

The liposomal membrane marker Rh-PE appeared in vesicular structures in the cell. The spectral analysis of several well-stained cells (Table 3) showed that about 75% of Rh-PE was colocalized with LysoTracker Red. Only a few Rh-PE stains that were almost exclusively arranged near the cell membrane (indicated by DiO staining) were not accompanied by this dye (Fig. 5C, black arrows).

FITC staining was found in vesicular structures and distributed diffusely in the cell. Figure 5D shows the typical distribution pattern of vesicular FITC-dextran, highlighting vesicular FITC-dextran and LysoTracker Red. DAPI and DiO are displayed in reduced colors. Only about 50% of the vesicular FITC-dextran was located in acidic compartments (Fig. 5D, green arrows). When comparing these results with those in Figure 5C and Table 3, one can see that most of these FITC-dextran-containing endosomes and lysosomes were also accompanied by Rh-PE.

However, the vesicular FITC staining was not always accompanied by Rh-PE and/or LysoTracker Red (Fig. 5C, white arrows), indicating that FITC-dextran-labeled liposomes can be taken up by a different mechanism than the Rh-PE-labeled liposomes. Only when FITC-dextran vesicles are accompanied by Rh-PE are they transported to acidic compartments. This can be explained by different surface properties of liposomes labeled with FITC (encapsulated) or Rh-PE (membrane incorporated).

In addition, in the image, only a few spots are stained exclusively with LysoTracker Red, indicating that not all acidic compartments contain liposomes (Fig. 5C, blue arrows).

DISCUSSION

In this study we describe a new, convenient method of color image analysis for use in endocytosis studies investigating the uptake and intracellular trafficking of lipo-

somes. For the first time, the spectral bio-imaging technology was successfully applied for this purpose in cell biology.

The fact that all dyes are measured simultaneously during the acquisition of the image makes the system efficient and easy to handle. A spectrum of light that emerges from the triple dichroic filter set (380–700 nm) is collected at each pixel of the image, which improves the accuracy of the results. The issue of accuracy of data acquisition and processing has been proven in a large number of publications that demonstrated the usage of the system for identifying various spectrally labeled probes by changing the results in comparison with single-color staining (42).

As demonstrated in our study, spectral bio-imaging with the SpectraCube system facilitates the decomposition of several, even strongly spectrally overlapping, dyes simultaneously in one measurement.

We demonstrated the correct signal resolution of five dyes in one image. FITC as a green dye and rhodamine as a red dye are often combined in double-staining experiments. Because the emission spectrum of FITC is very wide, its emission light also appears in the red fluorescence channel of rhodamine. This spectral overlap can easily result in false positive red fluorescence signals emitted by the green fluorescent dye FITC. In all fluorescent microscopic measurements including confocal microscopy, there is no possibility of accurately separating the green from the red signal when simultaneous excitation is used, unless a unique set of filters is developed that is adequate for the set of dyes being used. Such a method can work only on a microscope that has at least six filter cube positions and also needs an automated microscope. With sequential excitation of dyes and fine tuning of the excitation light intensity, one can achieve a strong reduction of this overlap in both methods. However, the spectrally resolved imaging method is superior to conventional fluorescent microscopic measurements because it distinguishes between the dyes by comparing the given reference spectra with the spectra of the pixels. We demonstrated not only the separation of a green and a red fluorescent dye but also the possibility of accurately sep-

arating two green fluorescent tracers with maxima differing by only 6 nm or two red fluorophores differing by only 10 nm.

Until now the SUN algorithm has been limited to the use of up to 10 fluorophores simultaneously. However, one has to be aware that an increasing number of fluorescent dyes could have an influence on the viability of the cell. For this reason, it is evident that the dye concentrations must be kept as low as possible.

A severe problem of some fluorescent dyes is strong photobleaching. The hardware-dependent, relatively long exposure time (up to 60–90s) requires the use of antifading substances to decrease bleaching effects. Further, the use of dyes with increased photostability reduces the drawback of long exposure times.

In our study we investigated the fate of pH-sensitive liposomes in COS-7 cells. Two different liposome preparations identical in lipid composition were labeled with hydrophilic FITC-dextran (encapsulated) or lipophilic Rh-PE (membrane incorporated). Whereas nearly all Rh-PE-labeled liposomes were delivered to acid organelles, only those FITC-dextran-labeled liposomes sharing the same fate were accompanied by Rh-PE.

As expected, part of the liposomal encapsulated FITC-dextran was found distributed diffusely in the cytoplasm of the cell, indicating that the marker was released from pH-sensitive liposomes and acidic organelles. However, a substantial amount of this dye still appeared in vesicular structures.

A remarkable finding was the appearance of vesicles stained exclusively with FITC-dextran. The absence of LysoTracker Red points to a caveolae-dependent uptake that has been described as the only endocytotic pathway without involving acidic compartments (43,44). Further, the absence of Rh-PE strongly suggests the existence of a sorting mechanism for the differently labeled liposomes on the cell surface, which determines different endocytotic pathways.

We conclude that there is a undeniable effect of Rh-PE on the uptake of particles that needs further elucidation and may be caused by the negative charge of the Rh-PE. Because both preparations contain a high amount of negatively charged lipids, the influence of the charge of Rh-PE plays a subordinate role. More significant might be the effect of the Rh-PE molecule itself: Rh-PE is a phospholipid that carries a bulky head-group label. This head-group label could interact as a ligand with cellular surface receptors triggering the receptor-mediated (clathrin-dependent) endocytosis.

The method of spectral bio-imaging offers an important tool for studying the uptake mechanisms and the intracellular routes and processing of (macro)molecules and particles in detail. With the possibility of using a variety of fluorescent dyes at the same time, particular organelles and cellular structures can be visualized. Localizing nucleolus, acidic compartments, cell membrane, mitochondria, Golgi apparatus, actin filaments, or microtubular structures while simultaneously following the fate of cell asso-

ciated and endocytosed material enables the investigation and understanding of cellular mechanisms.

ACKNOWLEDGMENTS

The authors gratefully acknowledge the critical reading of the manuscript by Roland Nitschke and Nir Katzir.

LITERATURE CITED

1. Gregoriadis G. Engineering liposomes for drug delivery: progress and problems. *Trends Biotechnol* 1995;13:527–537.
2. Lasic DD, Papahadjopoulos D. Medical applications of liposomes. New York: Elsevier; 1998.
3. Banerjee R. Liposomes: applications in medicine. *J Biomater Appl* 2001;16:3–21.
4. Düzgünes N, Nir S. Mechanisms and kinetics of liposome-cell interactions. *Adv Drug Deliv Rev* 1999;40:3–18.
5. Roth T, Porter K. Yolk protein uptake in the oocyte of the mosquito *Aedes aegypti*. *J Cell Biol* 1964;20:313–330.
6. Marsh M, McMahon HT. The structural era of endocytosis. *Science* 1999;285:215–220.
7. Apodaca G. Endocytic traffic in polarized epithelial cells: role of the actin and microtubule cytoskeleton. *Traffic* 2001;2:149–159.
8. Drummond DC, Zignani M, Leroux J. Current status of pH-sensitive liposomes in drug delivery. *Prog Lipid Res* 2000;39:409–460.
9. Lubrich B, van Calker D, Peschka-Süss R. Inhibition of inositol uptake in astrocytes by antisense oligonucleotides delivered by pH-sensitive liposomes. *Eur J Biochem* 2000;267:2432–2438.
10. Peschka-Süss R, Skalko-Basnet N. The association of plain and ligand-bearing neutral and pH-sensitive liposomes with various cells. *J Liposome Res* 2000;10:43–59.
11. Skalko N, Peschka R, Altenschmidt U, Lung A, Schubert R. pH-sensitive liposomes for receptor-mediated delivery to chicken hepatoma (LMH) cells. *FEBS Lett* 1998;434:351–356.
12. Brissou M, Tseng WC, Almonte C, Watkins S, Huang L. Subcellular trafficking of the cytoplasmic expression system. *Hum Gene Ther* 1999;10:2601–2613.
13. Collins D, Maxfield F, Huang L. Immunoliposomes with different acid sensitivities as probes for the cellular endocytic pathway. *Biochim Biophys Acta* 1989;987:47–55.
14. Parolin C, Zanotti G, Palu G. A model for the sequence-dependent DNA binding of 4',6-diamidino-2-phenylindole (DAPI). *Biochem Biophys Res Commun* 1995;208:332–338.
15. Poot M, Zhang YZ, Kramer JA, Wells KS, Jones LJ, Hanzel DK, Lugade AG, Singer VL, Haugland RP. Analysis of mitochondrial morphology and function with novel fixable fluorescent stains. *J Histochem Cytochem* 1996;44:1363–1372.
16. Vult von Steyern F, Josefsson JO, Tagerud S. Rhodamine B, a fluorescent probe for acidic organelles in denervated skeletal muscle. *J Histochem Cytochem* 1996;44:267–274.
17. Mason W. *Fluorescent and luminescent probes for biological activity*. London: Academic Press; 1993.
18. Spragg DD, Alford DR, Greferath R, Larsen CE, Lee KD, Gurtner GC, Cybulsky MI, Tosi PF, Nicolau C, Gimbrone MA Jr. Immunotargeting of liposomes to activated vascular endothelial cells: a strategy for site-selective delivery in the cardiovascular system. *Proc Natl Acad Sci USA* 1997;94:8795–8800.
19. Kono K, Igawa T, Takagishi T. Cytoplasmic delivery of calcein mediated by liposomes modified with a pH-sensitive poly(ethylene glycol) derivative. *Biochim Biophys Acta* 1997;1325:143–154.
20. Schrock E, du Manoir S, Veldman T, Schoell B, Wienberg J, Ferguson-Smith MA, Ning Y, Ledbetter DH, Bar-Am I, Soenksen D, Garini Y, Ried T. Multicolor spectral karyotyping of human chromosomes. *Science* 1996;273:494–497.
21. Speicher MR, Ballard SG, Ward DC. Karyotyping human chromosomes by combinatorial multi-fluor FISH. *Nat Genet* 1996;12:368–375.
22. Szuhai K, Bezrookove V, Wiegant J, Vrolijk J, Dirks RW, Rosenberg C, Raap AK, Tanke HJ. Simultaneous molecular karyotyping and mapping of viral DNA integration sites by 25-color COBRA-FISH. *Genes Chromosomes Cancer* 2000;28:92–97.
23. Becker W, Bergmann A, Biskup C, Zimmer T, Klocker N, Benndorf K. Multi-wavelength TCSPC lifetime imaging. *Proc SPIE* 2002;4620:79–84.
24. Farkas DL, Baxter G, DeBiasio RL, Gough A, Nederlof MA, Pane D, Pane J, Patek DR, Ryan KW, Taylor DL. Multimode light microscopy and the dynamics of molecules, cells, and tissues. *Annu Rev Physiol* 1993;55:785–817.

25. Malik Z, Cabib D, Buckwald RA, Talmi A, Garnini Y, Lipson SG. Fourier transform multipixel spectroscopy for quantitative cytology. *J Microsc* 1996;182:133-140.
26. Garini Y, Gil A, Bar-Am I, Cabib D, Katzir N. Signal to noise analysis of multiple color fluorescence imaging microscopy. *Cytometry* 1999; 35:214-226.
27. Goldstein SR, Kidder LH, Herne TM, Levin IW, Lewis EN. The design and implementation of a high-fidelity Raman imaging microscope. *J Microsc* 1996;184:35-45.
28. Ornberg RL, Woerner BM, Edwards DA. Analysis of stained objects in histological sections by spectral imaging and differential absorption. *J Histochem Cytochem* 1999;47:1307-1314.
29. Descour M, Volin C, Gleeson T, Dereniak E, Hopkins M, Wilson D, Maker P. Demonstration of a computed-tomography imaging spectrometer using a computer-generated hologram disperser. *Appl Opt* 1997;36:3694-3698.
30. Eils R, Uhrig S, Saracoglu K, Satzler K, Bolzer A, Petersen I, Chassery J, Ganser M, Speicher MR. An optimized, fully automated system for fast and accurate identification of chromosomal rearrangements by multiplex-FISH (M-FISH). *Cytogenet Cell Genet* 1998;82:160-171.
31. Tsurui H, Nishimura H, Hattori S, Hirose S, Okumura K, Shirai T. Seven-color fluorescence imaging of tissue samples based on Fourier spectroscopy and singular value decomposition. *J Histochem Cytochem* 2000;48:653-662.
32. Hope M, Bally M, Webb G, Cullis P. Production of large unilamellar vesicles by a rapid extrusion procedure. Characterization of size distribution and ability to maintain a membrane potential. *Biochim Biophys Acta* 1985;812:55-65.
33. Mayer LD, Hope MJ, Cullis PR. Vesicles of variable sizes produced by a rapid extrusion procedure. *Biochim Biophys Acta* 1986;858:161-168.
34. Bartlett G. Phosphorous assay in column chromatography. *J Biol Chem* 1959;234:466-468.
35. Florijn RJ, Slats J, Tanke HJ, Raap AK. Analysis of antifading reagents for fluorescence microscopy. *Cytometry* 1995;19:177-182.
36. Malik Z, Dishi M, Garini Y. Fourier transform multipixel spectroscopy and spectral imaging of protoporphyrin in single melanoma cells. *Photochem Photobiol* 1996;63:608-614.
37. Garini Y, Katzir N, Cabib D, Buckwald R, Soenksen D, Malik Z. Spectral bio-imaging. In: Wang X, Hermann B, editors. *Fluorescence imaging spectroscopy and microscopy*. New York: John Wiley & Sons; 1996. p 65-72.
38. Schrock E, Padilla-Nash H. Spectral karyotyping and multicolor fluorescence in situ hybridization reveal new tumor-specific chromosomal aberrations. *Semin Hematol* 2000;37:334-347.
39. Castleman KR, Eils R, Morrison L, Piper J, Saracoglu K, Schulze MA, Speicher MR. Classification accuracy in multiple color fluorescence imaging microscopy. *Cytometry* 2000;41:139-147.
40. White BH, Kaczmarek LK. Identification of a vesicular pool of calcium channels in the bag cell neurons of *Aplysia californica*. *J Neurosci* 1997;17:1582-1595.
41. Honig MG, Hume RI. Fluorescent carbocyanine dyes allow living neurons of identified origin to be studied in long-term cultures. *J Cell Biol* 1986;103:171-187.
42. Lu XY, Harris CP, Cooley L, Margolin J, Steuber PC, Sheldon M, Rao PH, Lau CC. The utility of spectral karyotyping in the cytogenetic analysis of newly diagnosed pediatric acute lymphoblastic leukemia. *Leukemia* 2002;16:2222-2227.
43. Mineo C, Anderson RG. Potocytosis. Robert Feulgen Lecture. *Histochem Cell Biol* 2001;116:109-118.
44. Shin JS, Abraham SN. Cell biology. Caveolae—not just craters in the cellular landscape. *Science* 2001;293:1447-1448.